IEEE Access
Multidisciplinary | Rapid Review | Open Access Journal

Received December 17, 2019, accepted January 6, 2020, date of publication January 20, 2020, date of current version February 11, 2020.

Digital Object Identifier 10.1109/ACCESS.2020.2968169

Physical Insights Into Cylindrical Illusion Device With Isotropic and Homogeneous Materials

ZHENZHONG YU, ZHONG YANG, YAN ZHANG, XINGLIU HU, AND YIZHI WANG
School of Intelligence Science and Control Engineering, Jinling Institute of Technology, Nanjing 211169, China

Corresponding authors: Zhenzhong Yu (nanfish@jit.edu.cn), Zhong Yang (yz@jit.edu.cn), and Xingliu Hu (xinghu8@163.com)

This work was supported in part by the Research Foundation of Jinling Institute of Technology under Grant JIT-B-201628, Grant Jit-rcyj-201604, and Grant Jit-fhxm-201906, in part by the University Science Research Project of Jiangsu Province under Grant 17KJB510021, in part by the Jiangsu Province's Natural Science Foundation under Grant BK20171114, and in part by the Production-Study Cooperative Education Project of the Ministry of Education Grant 201602009006.

ABSTRACT The cylindrical illusion device with isotropic and homogeneous materials is studied deeply based on the Mie scattering theory. The formula for illusion of core-shell structure is derived in the quasistatic approximation. Whether the inner core is a dielectric or PEC material, it can be equivalent to a certain target cylinder after wrapping a properly designed shell. We investigate what range of permittivity of the shell may be possible to achieve a target, which can provide convenient and intuitive design charts for an approximate design a core-shell illusion device. It is found that the number for the thickness of the shell is zero, one or two when the permittivities of the target and the shell take a variety of parameters. Moreover, the physical insights into the parameters' distribution are explained by analyzing the electric dipole moments in each part of the core-shell structure. It is interesting to see that a double negative material can be equivalently achieved by a PEC core coated with a positive magnetic material, which may offer a new design approach for the realization of double negative materials. The scattering widths and full-wave simulations are given to verify correctness of the proposed method.

INDEX TERMS Mie scattering, illusion device, full-wave simulations.

I. INTRODUCTION

Based on the form-invariance of Maxwell's equations under coordinate transformations, transformation optics (TO) has the potential ability to arbitrarily manipulate the propagation of the electromagnetic wave, resulting in many unconventional optical devices including invisibility cloak [1]–[4], illusion optical device [5]–[11], and so on. Invisibility cloak can guide light around the desired hidden region and make it come back to the original trajectory, which can be regarded as a special case of illusion device that can generate an illusion of free space. Lai *et al.* first presented the concept of illusion optics that can make an object appear like a different target object of some other shape and material makeup [5]. Illusion devices with various functionalities have also been proposed by using TO, including superscatterer, conversion device, shrinking device, ghost illusion device, source illusion device and so on [6]–[11]. The above mentioned illusion devices derived from TO are often composed of metamaterials with inhomogeneous anisotropic permittivity and permeability, which are difficult to realize especially in the optical range.

The associate editor coordinating the review of this manuscript and approving it for publication was Su Yan.

Another approach to manipulating the electromagnetic scattering is based on the scattering cancellation mechanism, first proposed by Alu and Engheta [12]–[14]. At the beginning, this approach is used to design the cloak. By covering a cloaked object with a layer of plasmonic shell, the scattering of the object with dimension much smaller than the wavelength can be drastically reduced. Moreover, this approach is not limited to design the cloak, but can also be applied to design the illusion device with the layered structure [15], [16]. For example, Yang *et al.* generalize the scattering cancellation method for the design of a spherical illusion device with isotropic and homogeneous materials [15]. We note that the single-shelled cylindrical illusion device with isotropic material has not been studied in depth. Recently, this simple core-shell nano-structure is used to exhibit substantial efficiency in terms of absorption, scattering and cloaking [17]–[19].

In this paper, we design cylindrical core-shell illusion devices composed of isotropic and homogeneous materials. The core cylinder is composed of common dielectric materials. Even the special case of perfectly conducting object is considered, in which the wave cannot penetrate. Two situations are considered. One is that a nonmagnetic or magnetic dielectric core covered by a well-designed shell

can be disguised as a nonmagnetic or magnetic target with different electromagnetic parameters, and the other is to make a PEC cylinder appear as a ε-negative material or a double-negative material. The radius ratios between target and core are chosen with different values respectively, and we analyze in detail what range of shell permittivity may be possible to achieve a target. In addition, the physical insights into the parameters' distribution are given by calculating the electric dipole moments of the core-shell structure immersed in a static electric field. The scattering widths and full-wave simulations are given to verify the correctness and effectiveness of the proposed design.

II. THEORETICAL FORMULATION

Let us consider the electromagnetic scattering from an infinite circular cylinder surrounded by one shell. The radius, permittivity and permeability of the core-shell structure are denoted as $(r_c, \varepsilon_c, \mu_c)$ and $(r_s, \varepsilon_s, \mu_s)$, respectively. An $e^{j\omega t}$-monochromatic plane wave is incident normally upon this cylindrical scatterer. Figure 1 shows that the core-shell structure with appropriate design can be disguised as another target cylinder with parameters $(r_t, \varepsilon_t, \mu_t)$.

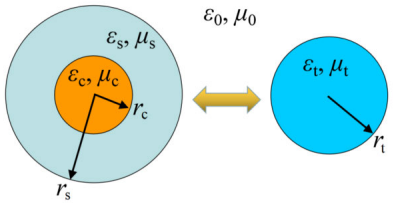

FIGURE 1. Schematic diagram of the cylindrical illusion problem. A core-shell structure with appropriate design can be disguised as another target cylinder with different parameters (r_t, ε_t, μ_t).

According to the Mie scattering theory, the scattered field in the cylindrical reference system can be expressed as the discrete sum of cylindrical Bessel functions with complex amplitudes c_n^{TM} and c_n^{TE}, respectively for TM and TE waves, which can be obtained by fulfilling the boundary conditions [20]. For simplicity, we consider the TM polarized wave in this paper. The expression for the TM wave can be written as [12]

$$c_n^{TM} = -\frac{\left|U_n^{TM}\right|}{\left|U_n^{TM}\right| + i\left|V_n^{TM}\right|} \tag{1}$$

where the quantities $\left|U_n^{TM}\right|$ and $\left|V_n^{TM}\right|$ are real valued for the lossless materials, and for the target cylinder $(r_t, \varepsilon_t, \mu_t)$ they can be expressed as

$$\left|U_{n\,(target)}^{TM}\right| = \begin{vmatrix} J_n(kr_t) & J_n(k_0 r_t) \\ \frac{k}{\varepsilon} J_n'(kr_t) & \frac{k_0}{\varepsilon_0}[J_n'(k_0 r_t)] \end{vmatrix} \tag{2}$$

$$\left|V_{n\,(target)}^{TM}\right| = \begin{vmatrix} J_n(kr_t) & -Y_n(k_0 r_t) \\ \frac{k}{\varepsilon} J_n'(kr_t) & -\frac{k_0}{\varepsilon_0} Y_n'(k_0 r_t) \end{vmatrix} \tag{3}$$

In equation (2) and equation (3), $k_0 = \omega\sqrt{\mu_0\varepsilon_0}$ and $k = \omega\sqrt{\mu_t\varepsilon_t}$ are the wave numbers in the free space and the target cylinder, respectively. J_n and Y_n are the Bessel functions of the first kind and the second kind. As in the case of the core-shell structure, $\left|U_n^{TM}\right|$ and $\left|V_n^{TM}\right|$ can be calculated as

$$\left|U_{n\,(core-shell)}^{TM}\right| = \begin{vmatrix} -J_n(k_c r_c) & J_n(k_s r_c) & Y_n(k_s r_c) & 0 \\ -\frac{k_c}{\varepsilon_c} J_n'(k_c r_c) & \frac{k_s}{\varepsilon_s} J_n'(k_s r_c) & \frac{k_s}{\varepsilon_s} Y_n'(k_s r_c) & 0 \\ 0 & J_n(k_s r_s) & Y_n(k_s r_s) & J_n(k_0 r_s) \\ 0 & \frac{k_s}{\varepsilon_s} J_n'(k_s r_s) & \frac{k_s}{\varepsilon_s} Y_n'(k_s r_s) & \frac{k_0}{\varepsilon_0} J_n'(k_0 r_s) \end{vmatrix} \tag{4}$$

$$\left|V_{n\,(core-shell)}^{TM}\right| = \begin{vmatrix} -J_n(k_c r_c) & J_n(k_s r_c) & Y_n(k_s r_c) & 0 \\ -\frac{k_c}{\varepsilon_c} J_n'(k_c r_c) & \frac{k_s}{\varepsilon_s} J_n'(k_s r_c) & \frac{k_s}{\varepsilon_s} Y_n'(k_s r_c) & 0 \\ 0 & J_n(k_s r_s) & Y_n(k_s r_s) & -Y_n(k_0 r_s) \\ 0 & \frac{k_s}{\varepsilon_s} J_n'(k_s r_s) & \frac{k_s}{\varepsilon_s} Y_n'(k_s r_s) & -\frac{k_0}{\varepsilon_0} Y_n'(k_0 r_s) \end{vmatrix} \tag{5}$$

where $k_c = \omega\sqrt{\mu_c\varepsilon_c}$ and $k_s = \omega\sqrt{\mu_s\varepsilon_s}$ are the wave numbers in the core and the shell. The scattered field is determined by the scattering coefficients $c_n^{TM}(|n| = 0, 1, 2, \ldots)$ up to a certain order N_{max}, and the subsequent coefficients can be negligible. Specially, when the radius of the cylindrical structure is much smaller than the working wavelength, namely quasistatic approximation, the scattering properties are dominated by the scattering term $|n| = 1$ corresponding to radiation from a dipole and the term $n = 0$ equivalent to an axial-directed magnetic line source. To achieve a good illusion performance with the simple core-shell structure, the quantities U_n^{TM} and V_n^{TM} for the core-shell illusion device and the target cylinder in the quasistatic condition should satisfy the following equation

$$\frac{\left|U_{n\,(target)}^{TM}\right|}{\left|V_{n\,(target)}^{TM}\right|} = \frac{\left|U_{n\,(core-shell)}^{TM}\right|}{\left|V_{n\,(core-shell)}^{TM}\right|}, \quad n = 0, 1. \tag{6}$$

When the size of the cylindrical scatterer becomes very small, equation (6) can be reduced to the following

$$\gamma_t^2(\mu_t - \mu_0) = -\gamma_s^2\mu_0 + \mu_c - \mu_s + \gamma_s^2\mu_s, \quad n = 0 \tag{7}$$

$$\begin{aligned} &\gamma_s^4(\varepsilon_c\varepsilon_0 - \varepsilon_c\varepsilon_s + \varepsilon_0\varepsilon_s - \varepsilon_s^2)(\varepsilon_0 + \varepsilon_t) \\ &\quad + \gamma_s^2(-\varepsilon_0\varepsilon_c - \varepsilon_s\varepsilon_c + \varepsilon_s\varepsilon_0 + \varepsilon_s^2)(\varepsilon_0 + \varepsilon_t) \\ &\quad - \gamma_t^2\gamma_s^2(\varepsilon_c\varepsilon_0 + \varepsilon_c\varepsilon_s + \varepsilon_0\varepsilon_s + \varepsilon_s^2)(\varepsilon_0 - \varepsilon_t) \\ &\quad - \gamma_t^2(-\varepsilon_0\varepsilon_c + \varepsilon_s\varepsilon_c + \varepsilon_s\varepsilon_0 - \varepsilon_s^2)(\varepsilon_0 - \varepsilon_t) = 0, \quad n = 1 \end{aligned} \tag{8}$$

where $\gamma_s = r_s/r_c$ and $\gamma_t = r_t/r_c$. As a special case of interest, when the cylinder core is perfectly conducting with electromagnetic parameters $\varepsilon_c = -j\infty$, $\mu_c = 0$,

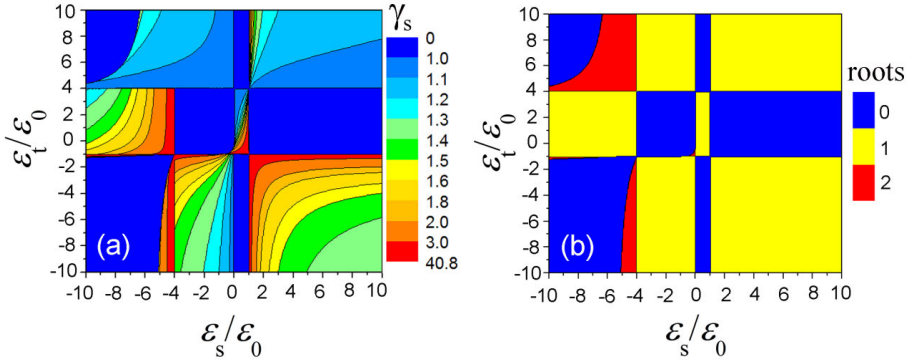

FIGURE 2. (a) Contour regions for the illusion condition in the ratio of $\gamma_t = 1$, for a dielectric cylinder with $\varepsilon_c = 4\varepsilon_0$. The blue regions represent the range of parameters for which the illusion condition cannot be fulfilled, whereas the colored regions show different values of γ_s that fulfill the condition. (b) The number of roots for γ_s. The blue regions represent the range of parameters for which the illusion condition has no roots, whereas the yellow and red regions correspond to one and two roots, respectively.

the condition for the illusion can be written as

$$\gamma_t^2(\mu_t - \mu_0) = -\gamma_s^2\mu_0 - \mu_s + \gamma_s^2\mu_s, \quad n = 0 \tag{9}$$

$$\gamma_s^4(\varepsilon_0 - \varepsilon_s)(\varepsilon_0 + \varepsilon_t) - \gamma_s^2(\varepsilon_0 + \varepsilon_s)(\varepsilon_0 + \varepsilon_t) - \gamma_t^2\gamma_s^2(\varepsilon_0 + \varepsilon_s)(\varepsilon_0 - \varepsilon_t) + \gamma_t^2(\varepsilon_s - \varepsilon_0)(\varepsilon_t - \varepsilon_0) = 0, \quad n = 1 \tag{10}$$

III. NUMERICAL EXAMPLES AND DISCUSSIONS

Equation (8) shows the relationship between the parameters $(\varepsilon_c, \varepsilon_s, \gamma_s)$ in the core-shell device and the parameters $(\varepsilon_t, \gamma_t)$ in the target cylinder. In order to visualize the equation (8), we plot a series of contour maps that show the function variation of γ_s, when varying the shell permittivity ε_s and the target permittivity ε_t, by setting several different values of γ_t. As the first example, we consider the inner core with permittivity $\varepsilon_c = 4\varepsilon_0$, and the radii of core and target are equal, namely $\gamma_t = 1$, shown in figure 2. The blue regions are those for which the corresponding values of ε_s and ε_t do not provide any physically reasonable value of γ_s in equation (8), i.e. for which illusion is not permissible. The contour plots provide a very intuitive understanding for designing a core-shell illusion device in the small-radii condition. Figure 2(b) shows the numbers of roots for the outer radius of shell. It can be seen that most of two-roots are distributed in the regions of $\{-4 > \varepsilon_s/\varepsilon_0 > -10,\ 10 > \varepsilon_t/\varepsilon_0 > 4\}$ and $\{-4 > \varepsilon_s/\varepsilon_0 > -10,\ -1 > \varepsilon_t/\varepsilon_0 > -10\}$, and only a small numbers of these are in the region of $\{0 > \varepsilon_s/\varepsilon_0 > -1,\ 0 > \varepsilon_t/\varepsilon_0 > -1\}$.

To provide physical insights into the parameters distribution shown in figure 2(a), we study the dipole moments in the core-shell structure. To begin with, we consider applying a static electric field $\boldsymbol{E}_0$ parallel to the cross section of the bare target cylinder, which can induce a dipole moment in the cylinder of unit length written as

$$\boldsymbol{p}_t = \pi r_t^2 \cdot 2\varepsilon_0 \frac{\varepsilon_t - \varepsilon_0}{\varepsilon_t + \varepsilon_0}\boldsymbol{E}_0 \tag{11}$$

We plot the normalized dipole moment $p_t' = (\varepsilon_t - \varepsilon_0)/(\varepsilon_t + \varepsilon_0)$ as a function of permittivity ε_t in figure 3. It shows that when the relative permittivity of cylinder is greater than -1, the normalized dipole moment increases gradually, but it is always less than 1. Among the region $-1 < \varepsilon_t/\varepsilon_0 < 1$, the direction of polarization is opposite to the direction of applied electric field. While the relative permittivity is less than -1, the normalized moment is always greater than 1, and the direction of the dipole is the same as that of the electric field. The normalized dipole moment tends to be infinite as the relative permittivity is in the vicinity of -1, corresponding to the localized surface plasmon resonance, namely an oscillating dipole mode. Moreover, it can be obtained from equation (11) that when the dielectric constant of the cylinder is reciprocal, the corresponding dipole moments have opposite values. In this case, the electromagnetic field produced by these dipoles with a phase difference of 180° is equal in magnitude and opposite in direction, but they have the same far-field scattering width. For example, the scattering by a cylinder with permittivity $\varepsilon_t = 5\varepsilon_0$ or $\varepsilon_t = 0.2\varepsilon_0$, shown in the figure 3(b). The far-field scattering widths are almost identical, however, strictly speaking, their scattering fields are different.

Then, we consider a core-shell structure placed in a uniform static electric field $\boldsymbol{E}_0$ along the $+x$ direction, which is perpendicular to the axis of the cylindrical structure. The electric field in each part of the structure can be determined by boundary conditions. The electric field in the core is a uniform field as

$$\boldsymbol{E}_c = -\frac{4r_s^2\varepsilon_s\varepsilon_0}{(\varepsilon_s-\varepsilon_c)(\varepsilon_s-\varepsilon_0)r_c^2-(\varepsilon_s+\varepsilon_c)(\varepsilon_s+\varepsilon_0)r_s^2}\boldsymbol{E}_0 \tag{12}$$

Then, the electric dipole moment in the core cylinder per unit length is calculated as

$$\boldsymbol{p}_c = \pi r_c^2\boldsymbol{P}_c = \pi r_c^2(\varepsilon_c - \varepsilon_0)\boldsymbol{E}_c = -\frac{4\pi r_s^2 r_c^2\varepsilon_s\varepsilon_0(\varepsilon_c-\varepsilon_0)}{(\varepsilon_s-\varepsilon_c)(\varepsilon_s-\varepsilon_0)r_c^2-(\varepsilon_s+\varepsilon_c)(\varepsilon_s+\varepsilon_0)r_s^2}\boldsymbol{E}_0 \tag{13}$$

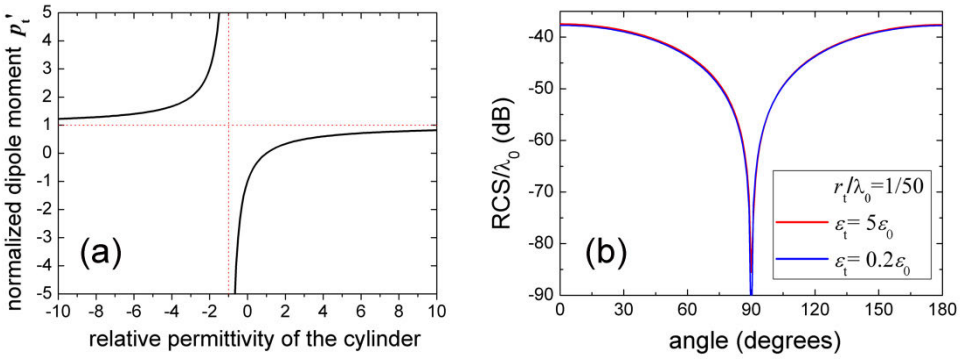

FIGURE 3. (a) The normalized dipole moment p_t' as a function of permittivity of the cylinder. (b) The scattering width normalized by wavelength for the cylinder $\varepsilon_t = 5\varepsilon_0$ (solid red line), and for the cylinder $\varepsilon_t = 0.2\varepsilon_0$ (solid blue line). The radius of the cylinder r_t is $\lambda_0/50$.

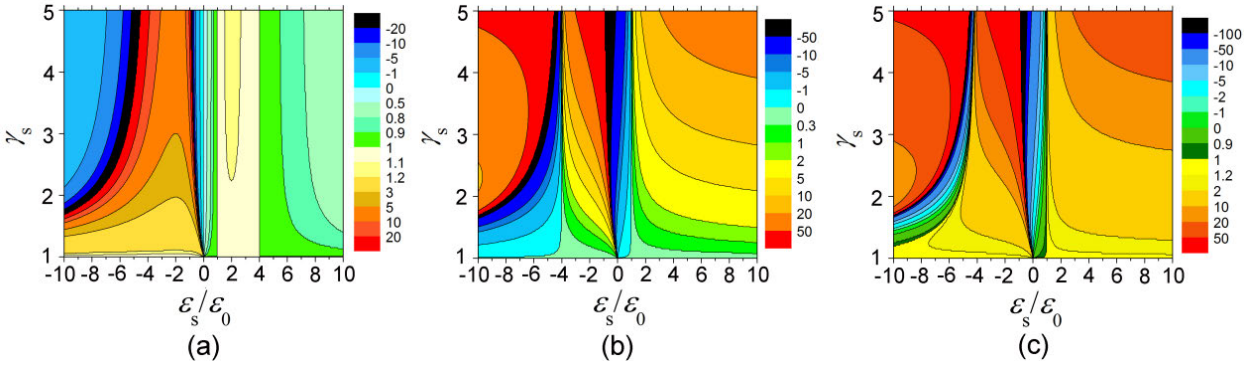

FIGURE 4. The core-shell structure with inner cylinder $\varepsilon_c = 4\varepsilon_0$ is considered. The normalized dipole moments in the core (a), in the shell (b), and the total moment (c) are a function of the permittivity of shell $\varepsilon_s/\varepsilon_0$ and the aspect ratio $\gamma_s = r_s/r_c$. All moments are normalized by that of the bare cylinder same as the core.

The electric field in the shell is not a uniform field, a function of (r, θ), and the component in the direction of applied electric field can be expressed as

$$\boldsymbol{E}_s = 2r_s^2\varepsilon_0\boldsymbol{E}_0\frac{[r^{-2}r_c^2(\varepsilon_s-\varepsilon_c)\cos 2\theta-(\varepsilon_c+\varepsilon_s)]}{(\varepsilon_s-\varepsilon_c)(\varepsilon_s-\varepsilon_0)r_c^2-(\varepsilon_s+\varepsilon_c)(\varepsilon_s+\varepsilon_0)r_s^2} \quad (14)$$

The electric dipole moment in the shell per unit length is along the direction of applied electric field, and can be expressed as

$$\begin{aligned}\boldsymbol{p}_s &= \iint_D \boldsymbol{P}_s ds = \iint_D (\varepsilon_s-\varepsilon_0)\boldsymbol{E}_s ds \\ &= \frac{2\pi(r_s^2-r_c^2)r_s^2\varepsilon_0(\varepsilon_c+\varepsilon_s)(\varepsilon_s-\varepsilon_0)\boldsymbol{E}_0}{(\varepsilon_s+\varepsilon_c)(\varepsilon_s+\varepsilon_0)r_s^2-(\varepsilon_s-\varepsilon_c)(\varepsilon_s-\varepsilon_0)r_c^2} \quad (15)\end{aligned}$$

where the integral region D is the cross section of the shell, and $\boldsymbol{P}_s$ is the electric polarization intensity along the applied electric field.

The total dipole moment in the core-shell structure can be obtained as

$$\begin{aligned}\boldsymbol{p}_{cs} &= \boldsymbol{p}_c + \boldsymbol{p}_s \\ &= 2\pi r_s^2\varepsilon_0\boldsymbol{E}_0\frac{[2\varepsilon_s(\varepsilon_c-\varepsilon_0)+(\gamma_s^2-1)(\varepsilon_c+\varepsilon_s)(\varepsilon_s-\varepsilon_0)]}{(\varepsilon_s+\varepsilon_c)(\varepsilon_s+\varepsilon_0)\gamma_s^2-(\varepsilon_s-\varepsilon_c)(\varepsilon_s-\varepsilon_0)} \quad (16)\end{aligned}$$

In order to make the core-shell structure appear like a target cylinder, the total dipole moments in the two cases should have the same value.

$$\boldsymbol{p}_{cs} = \boldsymbol{p}_t \quad (17)$$

After some calculations, we get the illusion condition the same as equation (8) derived from Mie scattering theory.

Next, we consider a cylinder with dielectric constant $\varepsilon_c = 4\varepsilon_0$ wrapped with a layer of material. Figure 4 shows each part and total electric dipole moments in the core-shell structure, as a function of the permittivity of shell ε_s and the aspect ratio $\gamma_s = r_s/r_c$. In the following analysis, we normalized all these dipole moments to the moment in the bare cylinder with $\varepsilon_c = 4\varepsilon_0$. The physical insights into the parameters'distribution are explained in the following points.

1) It can be seen that the electric dipole moment in the core increases slightly when the shell permittivity ε_s is between ε_0 and ε_c, whereas the moment decreases as the permittivity of the coating layer is greater than ε_c. When ε_s is greater than ε_0, the direction of the dipole in the shell is the same as that in the core, and the total dipole moment is larger than that of the bare cylinder. In this case, the moment of this core-shell structure can be equivalent to that of target cylinder with the

dielectric constant $\varepsilon_t > 4\varepsilon_0$ and $\varepsilon_t < -\varepsilon_0$, which can be concluded from figure 3(a). In figure 2(a), the similar conclusions can be obtained when the thickness of the shell is appropriately designed in the region of $\varepsilon_s > \varepsilon_0$. From the above, it is interesting to see that the core-shell structure with dielectric constants all greater than ε_0 can be equivalent to a material with negative dielectric constant, which provides a new and simple way to realize the equivalent scattering of nanoparticles with negative dielectric constant.

2) When dielectric constant of the shell is between 0 and ε_0, the dipole moment in the core decreases but with the same direction. However, the direction of the dipole moment in the shell is opposite to that in the core, therefore, the total dipole moment is smaller than that of the bare cylinder. With the increase of shell thickness and the decrease of dielectric constant ε_s, the total moment will further decrease and cause the opposite direction. From figure 3(a), we can conclude that when the dielectric constant of the coating is between 0 and ε_0, it can be equivalent to a bare cylinder with dielectric constant $4\varepsilon_0 > \varepsilon_t > -\varepsilon_0$ as shown in figure 2(a).
3) When dielectric constant of the shell is between -ε_0 and 0, the dipole moment in the core and shell will increase with the increase of shell's thickness, and a larger opposite moment will suddenly occur. Therefore, with the shell permittivity in the region $0 > \varepsilon_s > -\varepsilon_0$, this core-shell structure can be equivalent to a bare cylinder with dielectric constant $\varepsilon_t > 4\varepsilon_0$ and $\varepsilon_t < -\varepsilon_0$, and also to the dielectric constant little larger than $-\varepsilon_0$.
4) When dielectric constant of the shell is between $-4\varepsilon_0$ and $-\varepsilon_0$, the electric dipole moment in the core is larger than that of the bare cylinder of the same size. At the same time, the direction of moment in the shell is the same as that in the core, so the total moment is larger than that of the bare cylinder. Therefore, in this case the core-shell structure can be equivalent to a bare cylinder with permittivity $\varepsilon_t > 4\varepsilon_0$ and $\varepsilon_t < -\varepsilon_0$.
5) In the region $-4\varepsilon_0 > \varepsilon_s > -10\varepsilon_0$, the distribution of the total dipole moment is more complex, shown in figure 2(c). In the lower part of the region, the total dipole moment is larger than that of the same bare cylinder, so the core-shell structure can be equivalent to a target cylinder with dielectric constant of $\varepsilon_t > 4\varepsilon_0$ and $\varepsilon_t < -\varepsilon_0$. With the increase of thickness, the total dipole moment of the core-shell structure decreases gradually and changes direction, which can be equivalent to a target cylinder with dielectric constant $4\varepsilon_0 > \varepsilon_t > -\varepsilon_0$. Further increasing the thickness, the total moment is a large positive value equal to a bare cylinder with dielectric constant little smaller than $-\varepsilon_0$, and corresponds to the narrow strip near $\varepsilon_t = -\varepsilon_0$ in figure 2(a). It can be seen from figure 4 that in the region $-4\varepsilon_0 > \varepsilon_s > -10\varepsilon_0$, there may be two kinds of cladding layers with different thicknesses to achieve the same total moment, that is, the same target can be obtained by two design schemes. More intuitively, the root distribution of shell thickness is shown in figure 2(b).

According to the figure 2(a), when the core material is determined, the target cylinder with different material parameters can be achieved by changing the permittivity and thickness of the shell. In regions $\varepsilon_s > \varepsilon_0$ and $0 > \varepsilon_s > -4\varepsilon_0$, there is only one thickness of the shell to achieve a target cylinder. However, in region $\varepsilon_0 > \varepsilon_s > 0$, although there is only one root, the same far-field scattering width can be achieved by two shell thicknesses, due to the existence of reciprocal dielectric constants in this region. Finally, when the shell is in the interval $-4\varepsilon_0 > \varepsilon_s > -10\varepsilon_0$, there can be up to three shell thicknesses to achieve the same scattering width of the target cylinder. For instance, we choose $\varepsilon_s = -7.6\varepsilon_0$ and $\varepsilon_t = 5\varepsilon_0$, locating in the above interval with two thickness roots. The two outer radii are $r_s = 1.1008r_c$ and $r_s = 1.3314r_c$, respectively corresponding to the green and blue lines in the figure 5. Since the target cylinders with $\varepsilon_t = 0.2\varepsilon_0$ and $\varepsilon_t = 5\varepsilon_0$ have the same scattering cross widths under quasi-static condition, the outer radius of the shell corresponding to the target cylinder $\varepsilon_t = 0.2\varepsilon_0$ is calculated as $r_s = 1.6565r_c$, shown in the red line. It can be seen that the scattering cross widths of these properly designed core-shell structures almost coincide with that of the target cylinder.

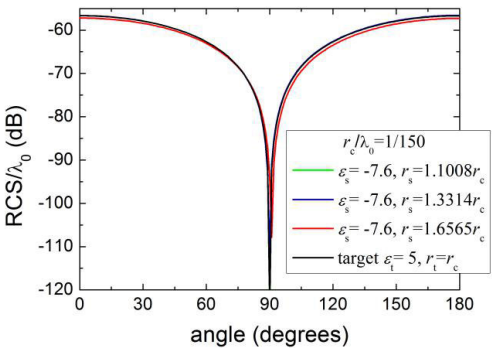

FIGURE 5. The normalized scattering widths of the core-shell structures with different shell thicknesses. We consider the permittivity of the core is $\varepsilon_c = 4\varepsilon_0$ and that of the shell is $\varepsilon_s = -7.6\varepsilon_0$. The target cylinder is $\varepsilon_t = 5\varepsilon_0$, $r_t = r_c$. The two roots of the shell are $r_s = 1.1008r_c$ (green line) and $r_s = 1.3314r_c$ (blue line), respectively. The outer radius of the core-shell structure corresponding to the cylinder $\varepsilon_t = 0.2\varepsilon_0$ is $r_s = 1.6565r_c$, shown in the red line. The scattering width of the target cylinder $\varepsilon_t = 5\varepsilon_0$ is also plotted in the figure for comparison (black line).

In the above, we discuss the case that the core and target cylinder are equal in size. In fact, the core-shell structure can give the same scattering response as the target of different sizes. Two contour maps for the illusion condition equation (8) in the ratio of $\gamma_t = 0.9$ and $\gamma_t = 1.2$ are plotted respectively, as shown in figures 6(a) and 6(b). Compared with figure 2(a) and figure 6(a), the obvious difference is that the dividing line changes from $\varepsilon_t = 4\varepsilon_0$ to $\varepsilon_t = 6.71\varepsilon_0$,

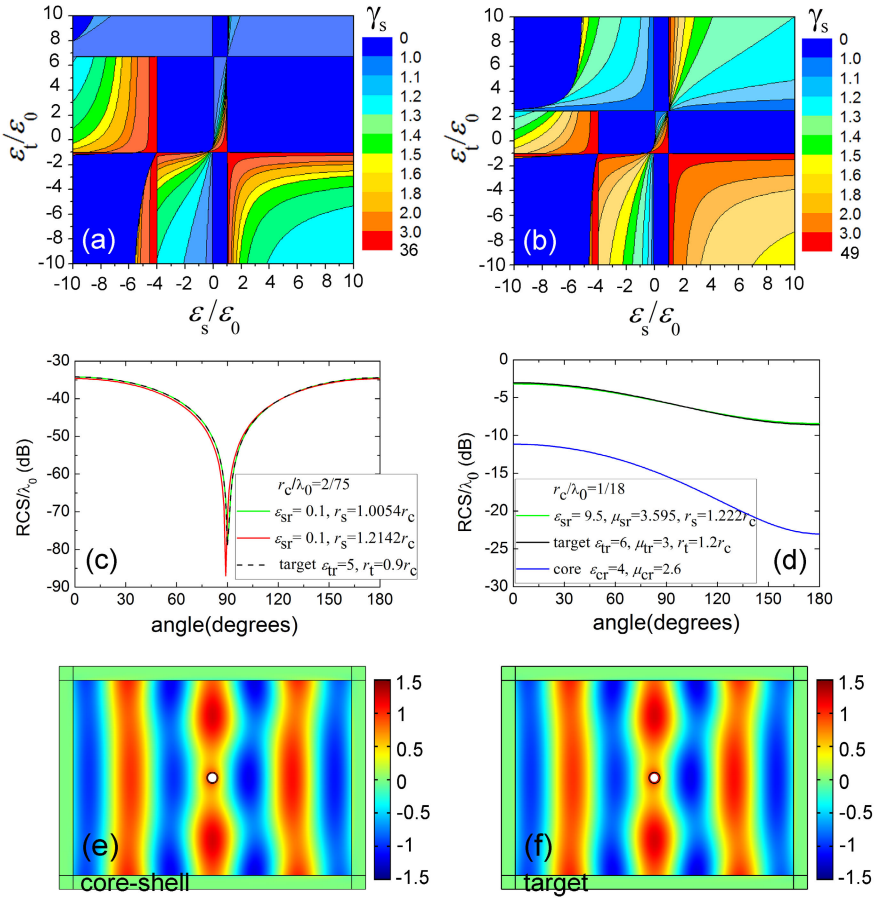

FIGURE 6. Contour regions for the illusion condition equation (8) in the ratio of $\gamma_t = 0.9$ (a) and $\gamma_t = 1.2$ (b), for an inner dielectric cylinder $\varepsilon_c = 4\varepsilon_0$. The blue regions represent the range of parameters for which the equation (8) cannot be fulfilled, whereas the colored regions show different values of γ_s that fulfill the equation (8). (c) The normalized scattering widths of two designed core-shell structures, and the target. We consider that the dielectric constant of the shell is $\varepsilon_s = \varepsilon_{sr}\varepsilon_0 = 0.1\varepsilon_0$ and the ratio is $\gamma_t = 0.9$ in figure 6(a). The outer radii of the shell corresponding to the target cylinders with $\varepsilon_t = \varepsilon_{tr}\varepsilon_0 = 5\varepsilon_0$ and $\varepsilon_t = \varepsilon_{tr}\varepsilon_0 = 0.2\varepsilon_0$ are calculated as $r_s = 1.0054r_c$ (solid green line) and $r_s = 1.2142r_c$ (solid red line), respectively. The scattering width of the target with $\varepsilon_t = 5\varepsilon_0$ and $r_t = 0.9r_c$ is also plotted for comparison (dashed black line). (d) A magnetic target is considered with parameters $\varepsilon_t = 6\varepsilon_0$, $\mu_t = 3\mu_0$ and $r_t = 1.2r_c$. The scattering width normalized by wavelength for the core-shell structure with $\varepsilon_s = 9.5\varepsilon_0$, $\mu_s = 3.595\mu_0$, $r_s = 1.222r_c$ (solid green line), and for the target cylinder with $\varepsilon_t = \varepsilon_{tr}\varepsilon_0 = 3\varepsilon_0$, $r_t = 1.2r_c$ (solid black line). The scattering width of the inner core with $\varepsilon_c = 4\varepsilon_0$, $\mu_c = 2.6\mu_0$ is also plotted for comparison (solid blue line). (e) The magnetic field distribution for the core-shell structure (solid green line) in figure 6(d). The white fleck in the cylinder shows the region where the values of magnetic field exceed the bounds. (f) The magnetic field distribution for the target (solid black line) in figure 6(d).

which can be explained by equation (11). By calculating, we get that the dipole moment of a cylinder with a dielectric constant of $\varepsilon_t = 4\varepsilon_0$ and a radius of $r_t = r_c$ is equivalent to that of a cylinder with $\varepsilon_t = 6.71\varepsilon_0$ and $r_t = 0.9r_c$. To demonstrate the illusion performance, we consider these parameters $\{\varepsilon_s = 0.1\varepsilon_0, \varepsilon_t = 5\varepsilon_0\}$ and $\{\varepsilon_s = 0.1\varepsilon_0, \varepsilon_t = 0.2\varepsilon_0\}$ having the same scattering widths, locating in the region $\{\varepsilon_0 > \varepsilon_s > 0, 6.71\varepsilon_0 > \varepsilon_t > -\varepsilon_0\}$. The outer radii of the shell corresponding to the target cylinders with $\varepsilon_t = 5\varepsilon_0$ and $\varepsilon_t = 0.2\varepsilon_0$ are calculated as $r_s = 1.0054r_c$ and $r_s = 1.2142r_c$, respectively. From figure 6(c), we can see that the scattering of two core-shell designs is basically the same as that of the target. For the case where the target is bigger than the core in the ratio of $\gamma_t = 1.2$, the dividing line now is $\varepsilon_t = 2.43\varepsilon_0$, shown in figure 6(b). The changes in this figure can also be explained by equation (11). Here, the magnetic target is investigated with $\varepsilon_t = 6\varepsilon_0$ and $\mu_t = 3\mu_0$, and the permeabiltiy of the inner core is set to $\mu_c = 2.6\mu_0$. We choose the permittivity of the shell as $\varepsilon_s = 9.5\varepsilon_0$, and then the outer radius and permeabiltiy of the shell are calculated as $r_s = 1.222r_c$ and $\mu_s = 3.595\mu_0$, according to equations (7) and (8). In figure 6(d), we can see that the normalized RCS of the core cylinder obviously increases after covering a well-designed shell, approximating to that of the target. To visually validate the illusion effect, full-wave EM simulation with the commercial COMSOL Mutiphysics

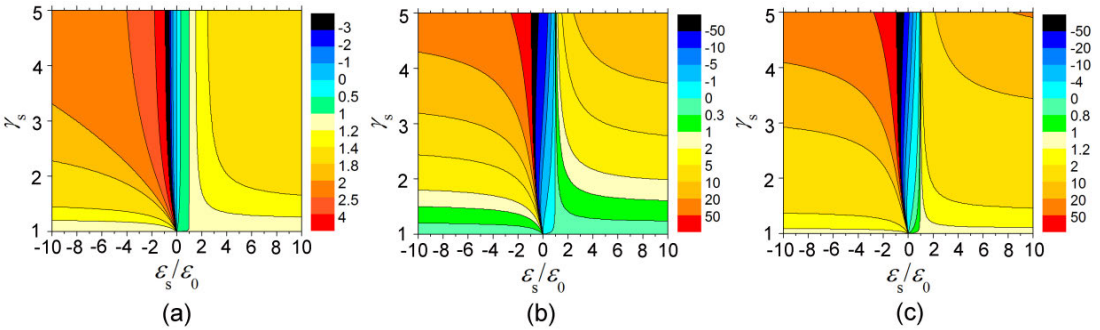

FIGURE 7. The core-shell structure with a PEC core is studied. The normalized dipole moments in the PEC core (a), in the shell (b), and the total moment (c) are a function of the shell's permittivity $\varepsilon_s/\varepsilon_0$ and the aspect ratio $\gamma_s = r_s/r_c$. All moments are normalized by that of a bare PEC cylinder same as the core.

package is carried out. A TM polarized plane wave (magnetic field normal to the simulation plane) with unit magnitude is incident horizontally from the left side. Figure 6(e) and (f) show the total magnetic field simulation of the core-shell structure and the target. The almost same distributions verify the effecitveness of the core-shell illusion device.

As a second example, we consider the core is a perfectly conducting cylinder in the core-shell structure. From equation (11) in the case of $\varepsilon_t = -j\infty$, we can obtain that the normalized dipole moment of a bare conducting cylinder is $p_t' = 1$, which is corresponding to the red horizontal dotted line in figure 3(a). It can be seen that the normalized moment of a bare conducting cylinder is between that of a cylinder with $\varepsilon_t < -\varepsilon_0$ and that of a cylinder with $\varepsilon_t > -\varepsilon_0$. Figure 7 shows each part and the total electric dipole moments in the core-shell structure constructed by a PEC cylinder wrapped with a layer of material. We normalized all these dipole moments to the moment in the PEC cylinder with a radius of r_t. The physical insights are briefly explained in the following points.

1) When the shell permittivity ε_s is larger than ε_0, the total moment is larger than that of the bare PEC cylinder shown in figure 7(c). Because the dipole moment of a cylinder with $\varepsilon_s < -\varepsilon_0$ is greater than that of a bare PEC cylinder with same size, the designed core-shell structure with $\varepsilon_s > \varepsilon_0$ can only be equivalent to a target cylinder with $\varepsilon_t < -\varepsilon_0$, shown in figure 8 (a).
2) In the region $\varepsilon_0 > \varepsilon_s > 0$, the total dipole moment is smaller than that of the bare PEC cylinder shown in figure 7(c). Therefore, in this case this designed core-shell structure can be equivalent to a target cylinder with $\varepsilon_t > -\varepsilon_0$ in figure 8(a).
3) In the region $0 > \varepsilon_s > -\varepsilon_0$, the total moment will increase with the increase of the shell's thickness, and a very large opposite moment will suddenly occur shown in figure 7(c). Therefore, in this region the core-shell structure can be equivalent to a target with $\varepsilon_t < -\varepsilon_0$, and also to a target with permittivity little larger than $-\varepsilon_0$, shown in figure 8(a).
4) In the region $-10\varepsilon_0 < \varepsilon_s < -\varepsilon_0$, the total moment is larger than that of the bare PEC cylinder, therefore the core-shell structure can be equivalent to the target cylinder with $\varepsilon_t < -\varepsilon_0$, shown in figures 7(c) and 8(a).

Figures 8(c) and 8(d) give two contour maps for the illusion condition equation (10) in the ratio of $\gamma_t = 1.2$ and $\gamma_t = 0.8$, respectively. In contrast to figure 8(a), a dividing line with $\varepsilon_t = 5.55\varepsilon_0$ appears in figure 8(c). The reason is as follows: the dipole moment of a bare PEC cylinder with a radius of r_c is equal to that of a dielectric cylinder with $\varepsilon_t = 5.55\varepsilon_0$ and $r_t = 1.2r_c$ by calculating equation (11). Therefore, when the permittivity of shell is in the region $\varepsilon_s > \varepsilon_0$, this core-shell structure can be equivalent to the target cylinder with the dielectric constant $\varepsilon_t > 5.55\varepsilon_0$ and $\varepsilon_t < -\varepsilon_0$. In figure 8 (d), dividing line with $\varepsilon_t = -4.56\varepsilon_0$ appears, the physical mechanism of which can also be explained by equation (11).

Figure 8(b) shows the root number of the shell's outer radius in the ratio of $\gamma_t = 1$. It can be clearly seen that there are two roots in the small region $\{0 > \varepsilon_s > -\varepsilon_0, 0 > \varepsilon_t > -\varepsilon_0\}$. Actually, when the permittivity of the shell is in the region $0 > \varepsilon_s > -\varepsilon_0$, there can be at most three kinds of core-shell structures to achieve the scattering width of the target. For example, we choose $\varepsilon_s = -0.1\varepsilon_0$ and $\varepsilon_t = -0.6\varepsilon_0$, and the two roots of the outer radius are $r_s = 1.573r_c$ and $r_s = 1.2715r_c$, respectively corresponding to the green line and the blue line in figure 9(a). Since the target cylinders with $\varepsilon_t = -0.6\varepsilon_0$ and $\varepsilon_t = -1.667\varepsilon_0$ have the same scattering widths under quasi-static condition, the outer radius of the shell corresponding to the target $\varepsilon_t = -1.667\varepsilon_0$ is calculated as $r_s = 1.0579r_c$. It can be seen in figure 9(a) that the core PEC material covered with non-magnetic materials cannot achieve the equivalent target. This is because in the case of the core-shell structure with a PEC core, the scattering is mainly composed of $n = 0$ and $n = \pm 1$ scattering terms under quasi-static condition, where $n = \pm 1$ corresponds to radiation from a dipole and $n = 0$ corresponds to a magnetic line source along the cylindrical axis. Using the designed nonmagnetic shell, we only obtain the same dipole scattering. The distribution difference of RCS in figure 9(a) is caused by the $n = 0$ scattering term. In order to make these three core-shell structures have the same $n = 0$ scattering term, we should adjust the permeabilities of the magnetic

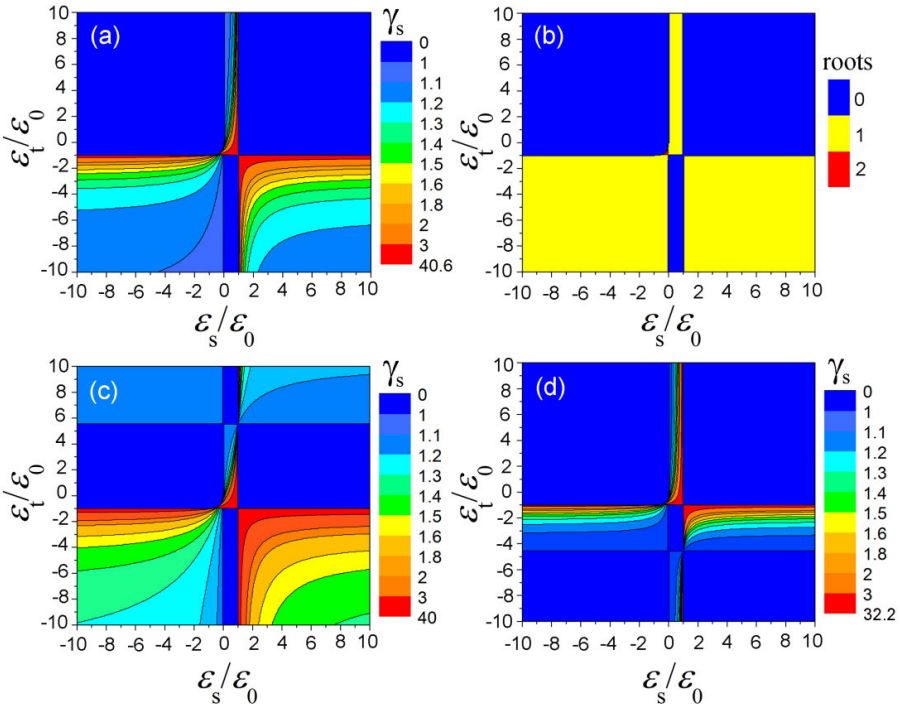

FIGURE 8. Contour regions for equation (10) in the ratio of $\gamma_t = 1$ (a), $\gamma_t = 1.2$ (c), and $\gamma_t = 0.8$ (d) with an inner PEC cylinder. The blue regions represent the range of parameters for which equation (10) cannot be fulfilled, whereas the colored regions show different values of γ_s that fulfill this equation. (b) The number of roots in equation (10) for γ_s in the ratio of $\gamma_t = 1$. The blue regions represent the thickness of the shell has no roots, whereas the yellow and red regions correspond to one and two roots, respectively.

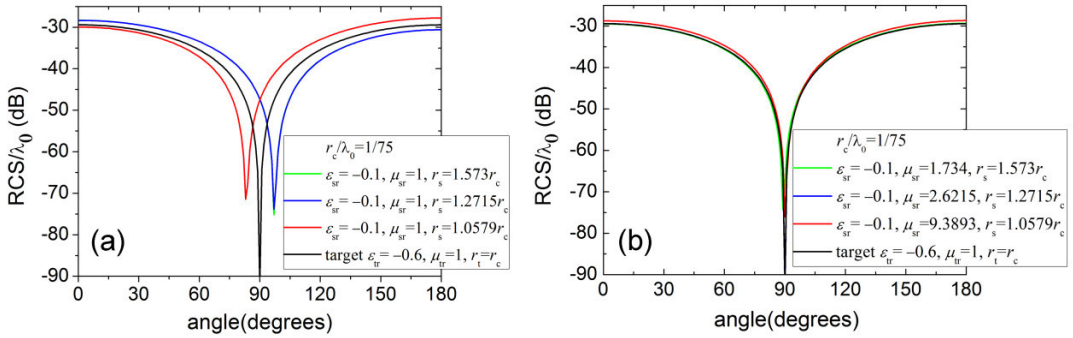

FIGURE 9. The normalized scattering widths of different core-shell structures are plotted. The PEC core and the target cylinder are equal in size. In figure 8(a), these parameters of $\varepsilon_s = \varepsilon_{sr}\varepsilon_0 = -0.1\varepsilon_0$ and $\varepsilon_t = \varepsilon_{tr}\varepsilon_0 = -0.6\varepsilon_0$ are selected. (a) The normalized RCSs for the nonmagnetic core-shell structures with outer radii $r_s = 1.573r_c$ (solid green line), $r_s = 1.2715r_c$ (solid blue line), and $r_s = 1.0579r_c$ (solid red line), respectively. The RCS of the target cylinder with $\varepsilon_t = \varepsilon_{tr}\varepsilon_0 = -0.6\varepsilon_0$ is also plotted for comparison (solid black line). (b) With the introduction of magnetic materials, the permeabilities of the magnetic shells are calculated as follows $\mu_s = \mu_{sr}\mu_0 = 1.734\mu_0$ (solid green line), $\mu_s = \mu_{sr}\mu_0 = 2.6215\mu_0$ (solid blue line), and $\mu_s = \mu_{sr}\mu_0 = 9.3893\mu_0$ (solid red line), respectively.

shells using equation (9), which are calculated as follows $\mu_s = 1.734\mu_0$, $\mu_s = 2.6215\mu_0$, and $\mu_s = 9.3893\mu_0$. With the introduction of magnetic materials, these RCS curves are almost identical to that of the nonmagnetic target cylinder shown in figure 9(b).

In the following, the target with a double negative material is investigated. For example, in the one-root region $\{\varepsilon_s > \varepsilon_0,\ \varepsilon_t < -\varepsilon_0\}$ in figure 8(a), we consider that permittivity of the shell is $\varepsilon_s = 5\varepsilon_0$ and the target is a left-handed material with electromagnetic parameters $\varepsilon_t = -2\varepsilon_0$ and $\mu_t = -0.5\mu_0$. According to equations (9) and (10), parameters of the shell are obtained as $r_s = 1.9471r_c$, $\mu_s = 0.8209\mu_0$. As can be seen from figure 10, RCS of the core-shell structure is very close to that of the target, and this is no longer a simple dipole scattering but including $n = 0$ and $n = \pm 1$ scattering terms. However, the scattering of

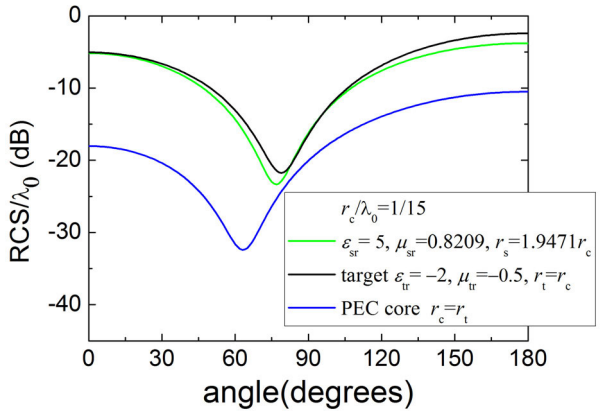

FIGURE 10. The normalized scattering widths of the designed core-shell structure, the target cylinder and the PEC core. The PEC core and the target cylinder are equal in size. In the one-root region $\{\varepsilon_s > \varepsilon_0, \varepsilon_t < -\varepsilon_0\}$ in figure 8(a), we consider that permittivity of the shell is $\varepsilon_s = \varepsilon_{sr}\varepsilon_0 = 5\varepsilon_0$ and the target is a left-handed material with electromagnetic parameters $\varepsilon_t = \varepsilon_{tr}\varepsilon_0 = -2\varepsilon_0$ and $\mu_t = \mu_{tr}\mu_0 = -0.5\mu_0$. The outer radius and the permeability of the shell are obtained as $r_s = 1.9471r_c$, $\mu_s = \mu_{sr}\mu_0 = 0.8209\mu_0$(solid green line). For comparison, the RCSs of the target cylinder and PEC core are also plotted.

the bare PEC core with $r_c = r_t$ is significantly different from the other two cases. To demonstrate the above design, full-wave EM simulation is carried out. Figure 11 illustrates the total and scattering magnetic field distributions in the near-field region. Perfect matched layers (PML) are chosen as the surrounding for the simulation region. In figure 11(a) and (b), the total fields are perturbed moderately with similar distributions. In order to compare the illusion effect more clearly, magnitudes of scattering magnetic field are plotted in figure 11(c) and (d). We compare the outside scattering field of the core-shell illusion device with that of the target cylinder, and find that the backscattering from the target is slightly bigger which is consistent with the RCS curves in figure 10. The above design indicates that the PEC core coated with a suitable magnetic material can be equivalent to a double negative material, which may offer a new design approach for the realization of double negative materials.

IV. CONCLUSION

We study the cylindrical illusion device using the core-shell structure with isotropic and homogeneous coating. The calculation formula for the core-shell illusion device in the quasistatic condition is derived. Whether the inner core is a dielectric or PEC material, it can be equivalent to a certain target cylinder after wrapping a designed shell. We use contour maps to visualize the corresponding relationship between the permittivities of the target and the shell, and give the corresponding thickness of shell. It is found that the root number for the thickness of the shell is zero, one or two in the different regions of the contour maps. Physical insights into the parameters' distribution are discussed by analyzing the electric dipole moments in the core-shell structure. In our calculation, the dimension of structure is much smaller than the wavelength, and the scattering properties are dominated by the monopole and dipole terms. For a big object, the higher order scattering contributions are becoming apparent, and a multilayered structure is needed to provide a good illusion performance. Optimization algorithm, which has been employed in invisibility cloak and other devices [21]-[25], will also be used to design the illusion device in the future work.

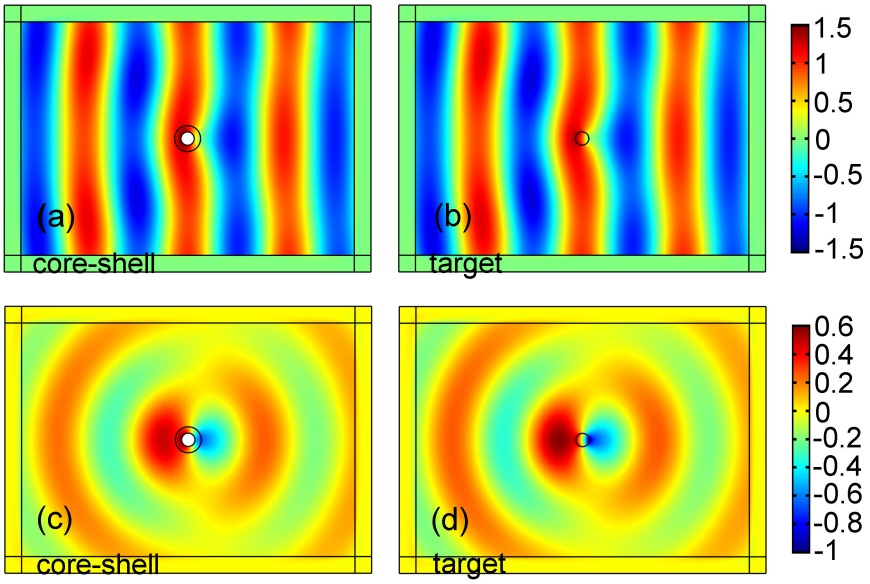

FIGURE 11. Full-wave simulations with the commercial COMSOL Mutiphysics package are carried out to test the core-shell illusion device in figure 10. A TM polarized plane wave with magnetic field normal to the simulation plane is incident horizontally from the left side. The total magnetic field distributions for the designed core-shell structure (a) and the target (b). Magnitudes of the scattering magnetic field from the designed core-shell structure (c) and the target (d).

REFERENCES

[1] J. B. Pendry, "Controlling electromagnetic fields," *Science*, vol. 312, no. 5781, pp. 1780–1782, Jun. 2006.
[2] H. Chen, B.-I. Wu, B. Zhang, and J. A. Kong, "Electromagnetic wave interactions with a metamaterial cloak," *Phys. Rev. Lett.*, vol. 99, Aug. 2007, Art. no. 063903.
[3] D. Schurig, J. J. Mock, B. J. Justice, S. A. Cummer, J. B. Pendry, A. F. Starr, and D. R. Smith, "Metamaterial electromagnetic cloak at microwave frequencies," *Science*, vol. 314, no. 5801, pp. 977–980, Nov. 2006.
[4] W. Cai, U. K. Chettiar, A. V. Kildishev, and V. M. Shalaev, "Optical cloaking with metamaterials," *Nature Photon.*, vol. 1, no. 4, pp. 224–227, Apr. 2007.
[5] Y. Lai, J. Ng, H. Y. Chen, D. Z. Han, J. J. Xiao, Z. Q. Zhang, and C. T. Chan, "Illusion optics: The optical transformation of an object into another object," *Phys. Rev. Lett.*, vol. 102, no. 25, Jun. 2009, Art. no. 253902.
[6] T. Yang, H. Chen, X. Luo, and H. Ma, "Superscatterer: Enhancement of scattering with complementary media," *Opt. Express*, vol. 16, no. 22, Oct. 2008, Art. no. 18545.
[7] W. X. Jiang, T. J. Cui, X. M. Yang, H. F. Ma, and Q. Cheng, "Shrinking an arbitrary object as one desires using metamaterials," *Appl. Phys. Lett.*, vol. 98, no. 20, May 2011, Art. no. 204101.
[8] W. X. Jiang, H. F. Ma, Q. Cheng, and T. J. Cui, "Virtual conversion from metal object to dielectric object using metamaterials," *Opt. Express*, vol. 18, no. 11, p. 11276, May 2010.
[9] W. X. Jiang, C.-W. Qiu, T. Han, S. Zhang, and T. J. Cui, "Creation of ghost illusions using wave dynamics in metamaterials," *Adv. Funct. Mater.*, vol. 23, no. 32, pp. 4028–4034, Aug. 2013.
[10] H. Chen, Y. Xu, H. Li, and T. Tyc, "Playing the tricks of numbers of light sources," *New J. Phys.*, vol. 15, no. 9, Sep. 2013, Art. no. 093034.
[11] X. F. Zang and C. Jiang, "Overlapped optics, illusion optics, and an external cloak based on shifting media," *J. Opt. Soc. Amer. B, Opt. Phys.*, vol. 28, no. 8, pp. 1994–2000, Aug. 2011.
[12] A. Alú and N. Engheta, "Achieving transparency with plasmonic and metamaterial coatings," *Phys. Rev. E, Stat. Phys. Plasmas Fluids Relat. Interdiscip. Top.*, vol. 72, no. 1, Jul. 2005, Art. no. 016623.
[13] A. Alú and N. Engheta, "Plasmonic materials in transparency and cloaking problems: Mechanism, robustness, and physical insights," *Opt. Express*, vol. 15, no. 6, p. 3318, Mar. 2007.
[14] A. Alú and N. Engheta, "Multifrequency optical invisibility cloak with layered plasmonic shells," *Phys. Rev. Lett.*, vol. 100, no. 11, p. 113901, Mar. 2008.
[15] F. Yang, Z. L. Mei, W. X. Jiang, and T. J. Cui, "Electromagnetic illusion with isotropic and homogeneous materials through scattering manipulation," *J. Opt.*, vol. 17, no. 10, Oct. 2015, Art. no. 105610.
[16] L. Zhang, Y. Shi, and C.-H. Liang, "Optimal illusion and invisibility of multilayered anisotropic cylinders and spheres," *Opt. Express*, vol. 24, no. 20, p. 23333, Oct. 2016.
[17] A. Sheverdin and C. Valagiannopoulos, "Core-shell nanospheres under visible light: Optimal absorption, scattering, and cloaking," *Phys. Rev. B, Condens. Matter*, vol. 99, no. 7, Feb. 2019, Art. no. 075305.
[18] A. Abrashuly and C. Valagiannopoulos, "Limits for absorption and scattering by core-shell nanowires in the visible spectrum," *Phys. Rev. A, Gen. Phys.*, vol. 11, no. 1, Jan. 2019, Art. no. 014051.
[19] D. C. Tzarouchis and A. Sihvola, "General scattering characteristics of resonant core–shell spheres," *IEEE Trans. Antennas Propag.*, vol. 66, no. 1, pp. 323–330, Jan. 2018.
[20] A. Alú D. Rainwater, and A. Kerkhoff, "Plasmonic cloaking of cylinders: Finite length, oblique illumination and cross-polarization coupling," *New J. Phys.*, vol. 12, no. 10, Oct. 2010, Art. no. 103028.
[21] Z. Z. Yu, Y. J. Feng, X. F. Xu, J. M. Zhao, and T. Jiang, "Optimized cylindrical invisibility cloak with minimum layers of non-magnetic isotropic materials," *J. Phys. D, Appl. Phys.*, vol. 44, no. 18, Apr. 2011, Art. no. 185102.
[22] Z. Z. Yu, Z. Yang, Y. H. Wang, H. F. Si, and G. S. Zhao, "Optimized cloaks made of near-zero materials for different-sized concealed targets," *Sci. Rep.*, vol. 8, Nov. 2018, Art. no. 16739.
[23] S. Xi, H. Chen, B. Zhang, B.-I. Wu, and J. A. Kong, "Route to low-scattering cylindrical cloaks with finite permittivity and permeability," *Phys. Rev. B, Condens. Matter*, vol. 79, Apr. 2009, Art. no. 155122.
[24] B. Ivsic, T. Komljenovic, and Z. Sipus, "Optimization of uniaxial multilayer cylinders used for invisible cloak realization," *IEEE Trans. Antennas Propag.*, vol. 58, no. 10, pp. 3397–3401, Oct. 2010.
[25] J. Peurifoy, "Nanophotonic particle simulation and inverse design using artificial neural networks," *Sci. Adv.*, vol. 4, no. 6, Jun. 2018, Art. no. eaar43206.

ZHENZHONG YU received the M.S. degree in electrical engineering from Southeast University, Nanjing, China, in 2008, and the Ph.D. degree in electromagnetic field and microwave technology from Nanjing University, Nanjing, in 2012. He is currently a Lecturer with the School of Intelligence Science and Control Engineering, Jinling Institute of Technology. His current research interests include electromagnetic scattering from the multilayered structure, surface plasmon polaritons, and artificial intelligence algorithm.

ZHONG YANG received the B.S., M.S., and Ph.D. degrees from Nanjing Aeronautics and Astronautics University, China, in 1991, 1993, and 1996, respectively. He is currently a Professor with the School of Intelligence Science and Control Engineering, Jinling Institute of Technology. His current interests are concentrate on intelligence science, control engineering, solar energy photovoltaic generating, and optical scattering.

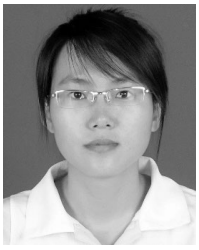

YAN ZHANG received the B.S. degree in mathematics and Ph.D. degree in automation from the Nanjing University of Science and Technology, Nanjing, China, in 2010 and 2015, respectively. She is currently a Lecturer with the School of Intelligence Science and Control Engineering, Jinling Institute of Technology. Her research interests include singular perturbation method, model predictive control, and optimal design in the electromagnetic device.

XINGLIU HU received the M.S. degree in automation and Ph.D. degree in intelligent control from the Nanjing University of Aeronautics and Astronautics, Nanjing, China, in 2004 and 2009, respectively. She is currently a Professor with the School of Intelligence Science and Control Engineering, Jinling Institute of Technology. Her current research interests include optical fiber sensor, optical materials, and intelligent control.

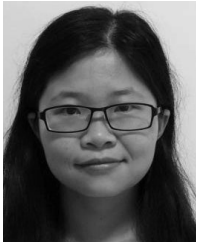

YIZHI WANG received the M.S. degree in system engineering from South Australia University, Adelaide, Australia, in 2011, and the Ph.D. degree in control engineering from the University of the West of England, Bristol, U.K., in 2018. She is currently a Lecturer with the School of Intelligence Science and Control Engineering, Jinling Institute of Technology. Her research interests include intelligent control, optimization algorithm in the application of electromagnetics, and fault diagnosis in industrial manufacture.